DOI:10.1021/cm901726s

CHEMISTRY OF MATERIALS
Article

Chemical Vapor Deposition of TiSi Nanowires on C54 $TiSi_2$ Thin Film: An Amorphous Titanium Silicide Interlayer Assisted Nanowire Growth

Huang-Kai Lin,[†] Hsin-An Cheng,[†] Chi-Young Lee,*[,‡] and Hsin-Tien Chiu*[,†]

[†]*Department of Applied Chemistry, National Chiao Tung University, Hsinchu, Taiwan 30050, R. O. C., and* [‡]*Department of Materials Science and Engineering and Center for Nanotechnology, Materials Science, and Microsystems, National Tsing Hua University, Hsinchu, Taiwan 30043, R. O. C.*

Received June 22, 2009. Revised Manuscript Received October 8, 2009

A C54-$TiSi_2$ film was grown on a Si substrate at 1073 K by low pressure chemical vapor deposition (LPCVD) employing titanium subchlorides $TiCl_{x(g)}$, generated by reacting between $TiCl_{4(g)}$ and $Ti_{(s)}$ at 1173 K, as the Ti source. Growth of titanium silicide (TiSi) nanowires (NWs; diameter 30−80 nm, length several micrometers) on a C54-$TiSi_2$ film was observed. Growth direction of the NWs was determined to be along the [010] axis. An amorphous titanium silicide interlayer was observed between the NWs and the C54-$TiSi_2$ film. This interlayer, probably existing as a quasi-liquid thin film during the growth, appears to be the key factor to assist the NW development. Field emission properties, turn-on field E_o and field enhancement factor β, of the vertically grown TiSi NWs were determined to be 5.25 V μm^{-1} and 876, respectively.

1. Introduction

Metal silicides, including silicides of Ti, Cr, Fe, Co, and Ni, are intensively investigated because their unique physical and chemical properties could meet the requirements of modern technological applications.[1] Among the silicides, titanium silicides show high thermal stability, low electrical resistivity, low work function, and low density.[1−4] These properties make titanium silicides good candidates for enhanced electronic field emission source, field ionization source, interconnect in nanoelectronics, and solar energy assisted catalytic water splitting.[5−10] For many metal silicides, varying the synthesis conditions could alter the metal to silicon composition ratio and the crystal phase. Consequently, properties of the silicides are changed as well. Thus, it is possible to prepare silicide samples with diverse properties within one reaction system. For titanium silicides, there are six reported phases, including C54-$TiSi_2$, C49-$TiSi_2$, TiSi, Ti_5Si_4, Ti_5Si_3, and Ti_3Si.[11,12] Among them, C54-$TiSi_2$ is the most studied for its applications in microelectronic devices. C54-$TiSi_2$ has a low electrical resistivity 10−28 $\mu\Omega$cm and a high melting point 1773 K.[1,2,13] The other disilicide C49-$TiSi_2$, with a higher electrical resistivity ca. 100 $\mu\Omega$cm, is considered to be a low temperature metastable phase before the formation of C54-$TiSi_2$.[14] Ti_5Si_3 is a promising high temperature material for protective refractory coating because of its high melting point 2403 K, excellent creep resistance, and high oxidation resistance.[1,15−17] For the remaining silicides TiSi, Ti_5Si_4, and Ti_3Si, applications were seldom reported due to the difficulties of preparing them in pure phases.[2,18−24] For example, Ti_3Si has rarely been described in related research because it is easily destabilized by oxygen in the processing. TiSi is another silicide with limited reports. In contrast to Ti_3Si,

*Corresponding author. E-mail: cylee@mx.nthu.edu.tw (C.-Y.L.); htchiu@faculty.nctu.edu.tw (H.-T.C.).

(1) Maex, K.; Rossum, M. V. *Properties of Metal Silicides*; IEE: London, 1995.
(2) Murarka, S. P.; Fraser, D. B. *J. Appl. Phys.* **1980**, *51*, 350.
(3) Murarka, S. P. *Silicides for VLSI Applications*; Academic Press: Orlando, FL, 1983.
(4) Bucher, E.; Schultz, S.; Lux-Steiner, M. C.; Munz, P.; Gubler, U. G. F. *Appl. Phys. A* **1986**, *40*, 71.
(5) Xiang, B.; Wang, Q.-X.; Wang, Z.; Zhang, X.-Z.; Liu, L.-Q.; Xu, J.; Yu, D.-P. *Appl. Phys. Lett.* **2005**, *86*, 243103.
(6) Chang, C.-M.; Chang, Y.-C.; Lee, C.-Y.; Yen, P.-H.; Lee, W.-F.; Chen, L.-J. *J. Phys. Chem. C* **2009**, *113*, 9153.
(7) Riley, D. J.; Mann, M.; MacLaren, D. A.; Dastoor, P. C.; Allison, W. *Nano Lett.* **2003**, *3*, 1455.
(8) Singh, J. P.; Karabacak, T.; Lu, T. M.; Wang, G. C.; Koratkar, N. *Appl. Phys. Lett.* **2004**, *85*, 3226.
(9) Ritterskamp, P.; Kuklya, A.; Wustkamp, M.-A.; Kerpen, K.; Weidenthaler, C.; Demuth, M. *Angew. Chem., Int. Ed.* **2007**, *46*, 7770.
(10) Li, Q.; Lu, G. *Catal. Lett.* **2008**, *125*, 376.
(11) Massalski, T. B.; Okamoto, H.; Subramanian, P. R.; Kacprzak, L. *Binary Alloy Phase Diagrams*; American Society for Metals: Metals Park, OH, 1990.
(12) Beyers, R.; Sinclair, R. *J. Appl. Phys.* **1985**, *57*, 5240.
(13) Murarka, S. P.; Fraser, D. B. *J. Appl. Phys.* **1980**, *51*, 342.
(14) Mann, R. W.; Clevenger, L. A. *J. Electrochem. Soc.* **1994**, *141*, 1347.
(15) Willams, J. J.; Akinc, M. *Oxid. Met.* **2002**, *58*, 57.
(16) Zhang, L.; Wu, J. *Acta Mater.* **1998**, *46*, 3535.
(17) Shah, D. M.; Berczik, D.; Anton, D. L.; Hecht, R. *Mater. Sci. Eng., A* **1992**, *155*, 45.
(18) Yen, B. K.; Aizawa, T.; Kihara, J. *J. Am. Ceram. Soc.* **1998**, *81*, 1953.
(19) Doppiu, S.; Monagheddu, M.; Cocco, G. *J. Mater. Res.* **2001**, *16*, 1266.
(20) Bentini, G. G.; Nipoti, R.; Armigliato, A.; Berti, M.; Drigo, A. V.; Cohen, C. *J. Appl. Phys.* **1985**, *57*, 270.
(21) Clevenger, L. A.; Cabral, C.; Roy, R. A.; Lavoie, C.; JordanSweet, J.; Brauer, S.; Morales, G.; Ludwig, K. F.; Stephenson, G. B. *Thin Solid Films* **1996**, *289*, 220.
(22) Wakelkamp, W. J. J.; Loo, F. J. J. V.; Metselaar, R. *J. Eur. Ceram. Soc.* **1991**, *8*, 135.
(23) Cockeram, B.; Wang, G. *Thin Solid Films* **1995**, *269*, 57.
(24) Ramos, A. S.; Nunes, C. A.; Coelho, G. C. *Mater. Charact.* **2006**, *56*, 107.

Published on Web 10/21/2009

TiSi may have interesting applications because it has a high melting point 1843 K, a low electrical resistivity 60 $\mu\Omega$cm, and one of the highest mechanical hardness (Hμ) 18.0 among all titanium silicides.[1,3,25] Nonetheless, to this date, methods to fabricate TiSi in quantities suitable for extensive studies are limited.[22,26−28] Thus, searching for new techniques to synthesize TiSi is important in silicide research. In general, three types of techniques are commonly employed to prepare titanium silicides. The first type is powder based methods. These include arc melting and self-propagating exothermic reactions, such as ball milling, shock loading, and thermal ignition of stoichiometric mixtures of elemental powders.[18] The second one is physical vapor deposition (PVD) processes. They are frequently used to grow titanium silicide thin films. A well-known example is the salicide process.[13,29,30] It includes two steps, evaporation of Ti or coevaporation of Ti and Si atoms onto Si substrates, followed by annealing the as-deposited thin film at a high temperature to form silicides. The last one is chemical vapor deposition (CVD) reactions. By reacting $TiCl_4$ with silane or silicon chlorides at high temperatures, titanium silicide thin films can be grown.[21,31−33] CVD provides possibilities to prepare kinetically stable phases which are difficult to obtain using the other methods. Recently, by employing variations of the fabrication methods mentioned above, preparations of nanosized one-dimensional (1D) silicides of Ti, V, Cr, Mn, Fe, Co, Ni, and Ta have been reported.[5,6,34−60] For titanium silicides, these include nanowires (NWs) of TiSi and C54-$TiSi_2$, nanopins (NPs) of TiSi, nanobats of Ti_5Si_4, and nanonets (NNs) of C49-$TiSi_2$, as listed in Table 1.[5,6,34,35,37,38] Previously, we have communicated the growth of Ti_5Si_3 NWs on top of C54-$TiSi_2$ thin films grown by reacting titanium subhalides $TiCl_{x(g)}$, generated by passing $TiCl_{4(g)}$ over $Ti_{(s)}$ at 1173 K, with Si substrates in a CVD process.[36] Herein, we wish to report our further investigation on this unique titanium silicide fabrication process. We have discovered that in addition to Ti_5Si_3 NWs, dense TiSi NW arrays can be grown by this process after adjusting the reaction parameters. In addition, this study shows the existence of an amorphous $TiSi_{2-x}$ layer between the NWs and the C54-$TiSi_2$ film below them. Importance of the amorphous $TiSi_{2-x}$ layer to the NW growth and electron field emission (EFE) properties of the NW array will also be discussed.

2. Experimental Section

2.1. Growth of Titanium Silicide Samples. Thin films and NWs of titanium silicide samples were grown by a low pressure CVD (LPCVD) using a horizontal hot-wall quartz tube reactor heated by a three-zone tube furnace (Lindberg 55346), as shown in Figure S1 in the Supporting Information. Si (100) (n-type, 0.7 cm × 1.5 cm × 0.525 mm) wafers, pretreated by a standard RCA cleaning process, were placed at the center inside the reactor, which was at zone 2. Ti powders (0.4 g, Aldrich 99.7%) in a quartz boat were placed at zone 1, which was upstream from the Si substrates. To reduce O_2 and H_2O partial pressures, the reactor was first purged with Ar then evacuated below 0.4 Pa before the reaction began. After zone 1 was heated to 1173 K and zone 2 reached 973−1073 K, $TiCl_4$ (Fluka 99%) kept at 298 K was vaporized into the reactor. The evaporation of $TiCl_4$ was controlled at a pressure of 2.67 Pa for 10 min to 6 h, depending on the experiments, by a low-flow metering needle valve (Swagelok, SS-SS4). The amount of $TiCl_4$ introduced was 0.42 mL/h. Assuming that the evaporation rate was constant, the flow rate of the $TiCl_4$ was estimated to be 12 mg/min (0.063 mmol/min). After the vaporization was stopped, the furnace was allowed to cool to room temperature. Deposition of gray to black films on the wafers was observed. Detailed

(25) Fouad, O. A.; Yamazato, M.; Nagano, M. *Appl. Surf. Sci.* **2002**, *195*, 130.
(26) Brukl, C.; Nowotny, H.; Schob, O.; Benesovsky, F. *Monatsh. Chem.* **1961**, *92*, 781.
(27) Samsonov, G. V.; Okhremchuk, L. N.; Podgrushko, N. F.; Podchernyaeva, I. A.; Fomenko, V. S. *Inorg. Mater.* **1976**, *12*, 720.
(28) Kosolapova, T. Y. *Handbook of High Temperature Compounds: Properties, Production, Applications*; Hemisphere Publishing Corporation: New York, 1990.
(29) Chopra, K. L. *Thin Film Phenomena*; McGraw-Hill: New York, 1969.
(30) Hoffman, D. W.; Thronton, J. A. *Thin Solid Films* **1977**, *40*, 355.
(31) Yim, W. M.; Stotko, E. J. *J. Electrochem. Soc.* **1974**, *121*, 965.
(32) Hallais, J. P.; Boccon-Gibod, D.; Chane, J. P.; Durand *J. Electrochem. Soc.* **1977**, *124*, 1290.
(33) Lacombe, J.; Duchemin, J. P.; Bonnet, M.; Huyghe, D. *Electron. Lett.* **1977**, *13*, 472.
(34) Du, J.; Du, P.-Y.; Hao, P.; Huang, Y.-F.; Ren, Z.-D.; Han, G.-R.; Weng, W.-J.; Zhao, G.-L. *J. Phys. Chem. C* **2007**, *111*, 10814.
(35) Du, J.; Ren, Z.-D.; Tao, K.-Y.; Hu, A.-H.; Hao, P.; Huang, Y.-F.; Zhao, G.-L.; Weng, W.-J.; Han, G.-R.; Du, P.-Y. *Cryst. Growth Des.* **2008**, *8*, 3543.
(36) Lin, H.-K.; Tzeng, Y.-F.; Wang, C.-H.; Tai, N.-H.; Lin, I.-N.; Lee, C.-Y.; Chiu, H.-T. *Chem. Mater.* **2008**, *20*, 2429.
(37) Zhou, S.; Liu, X.-H.; Lin, Y.-J.; Wang, D.-W. *Angew. Chem., Int. Ed.* **2008**, *47*, 7681.
(38) Zhou, S.; Liu, X.-H.; Lin, Y.-J.; Wang, D.-W. *Chem. Mater.* **2009**, *21*, 1023.
(39) In, J.; Seo, K.; Lee, S.; Yoon, H.; Park, J.; Lee, G.; Kim, B. *J. Phys. Chem. C* **2009**, *113*, 12996.
(40) Seo, K.; Varadwaj, K. S. K.; Cha, D.; In, J.; Kim, J.; Park, J.; Kim, B. *J. Phys. Chem. C* **2007**, *111*, 9072.
(41) Szczech, J. R.; Schmmitt, A. L.; Bierman, M. J.; Jin, S. *Chem. Mater.* **2007**, *19*, 3238.
(42) Zhou, F.; Szczech, J.; Pettes, M. T.; Moore, A. L.; Jin, S.; Shi, L. *Nano Lett.* **2007**, *7*, 1649.
(43) Higgins, J. M.; Schmitt, A. L.; Guzei, L. A.; Jin, S. *J. Am. Chem. Soc.* **2008**, *130*, 16086.
(44) Ham, M.-H.; Lee, J.-W.; Moon, K.-J.; Choi, J.-H.; Myoung, J.-M. *J. Phys. Chem. C* **2009**, *113*, 8143.
(45) Quyang, L.; Thrall, E. S.; Deshmukh, M. M.; Park, H. *Adv. Mater.* **2006**, *18*, 1437.
(46) Schmitt, A. L.; Bierman, M. J.; Schmeisser, D.; Himpsel, F. J.; Jin, S. *Nano Lett.* **2006**, *6*, 1617.
(47) Varadwaj, K. S. K.; Seo, K. I., J.; Mohanty, P.; Park, J.; Kim, B. *J. Am. Chem. Soc.* **2007**, *129*, 8594.
(48) Schmitt, A. L.; Zhu, L.; Schmeiber, D.; Himpsel, F. J.; Jin, S. *J. Phys. Chem. B* **2006**, *110*, 18142.
(49) Seo, K.; Varadwaj, K. S. K.; Mohanty, P.; Lee, S.; Jo, Y.; Jung, M.-H.; Kim, J.; Kim, B. *Nano Lett.* **2007**, *7*, 1240.
(50) Seo, K.; Lee, S.; Yoon, H.; In, J.; Varadwaj, K. S. K.; Jo, Y.; Jung, M. H.; Kim, J.; Kim, B. *ACS Nano* **2009**, *3*, 1145.
(51) Decker, C. A.; Solanki, R.; Freeouf, J. L.; Carruthers, J. R.; Evans, D. R. *Appl. Phys. Lett.* **2004**, *84*, 1389.
(52) Kim, J.; Anderson, W. A. *Thin Solid Films* **2005**, *483*, 60.
(53) Kim, J.; Anderson, W. A.; Song, Y. J.; Kim, G. B. *Appl. Phys. Lett.* **2005**, *86*, 253101.
(54) Song, Y.; Jin, S. *Appl. Phys. Lett.* **2007**, *90*, 173122.
(55) Song, Y.; Schmitt, A. L.; Jin, S. *Nano Lett.* **2007**, *7*, 965.
(56) Kim, C.-J.; Kang, K.; Woo, Y. S.; Ryu, K.-G.; Moon, H.; Kim, J.-M.; Zang, D.-S.; Jo, M.-H. *Adv. Mater.* **2007**, *19*, 3637.
(57) Kim, J.; Shin, D. H.; Lee, E.-S.; Han, C.-S.; Park, Y. C. *Appl. Phys. Lett.* **2007**, *90*, 253103.
(58) Kang, K.; Kim, S.-K.; Kim, C.-J.; Jo, M.-H. *Nano Lett.* **2008**, *8*, 431.
(59) Lee, C. Y.; Lu, M. P.; Liao, K. F.; Lee, W. F.; Huang, C. T.; Chen, S. Y.; Chen, L. J. *J. Phys. Chem. C* **2009**, *113*, 2286.
(60) Chueh, Y.-L.; Ko, M.-T.; Chou, L.-J.; Chen, L.-J.; Wu, C.-S.; Chen, C.-D. *Nano Lett.* **2006**, *6*, 1637.

Table 1. Summary of Titanium Silicide Samples

reference sample	process, product, morphology, and phase	NWs length/ film thickness	growth conditions: temperature (K)	growth conditions: time (min)	E_o (V μm^{-1})	β	J_{max} (μA cm^{-2})
ref 5	PVD (Ti powder/Si wafer) C54-$TiSi_2$ NWs	tens to hundred micrometers	1073	180	8	501	0.23
ref 6	PVD (Si powder/Ti foil) Ti_5Si_4 Nanobat	350 nm	1073	180	1.47[a]	1350	0.36
ref 35	CVD ($TiCl_4$, SiH_4/borosilicate) TiSi NPs and NWs on Ti_5Si_3 film	0.7−1 μm/2 μm	963−1023	1−36	–[b]	–[b]	–[b]
ref 37	CVD ($TiCl_4$, SiH_4/Si wafer) C49-$TiSi_2$ Nanonet	2−10 μm	948	15	–[b]	–[b]	–[b]
ref 38	CVD ($TiCl_4$, SiH_4/Si wafer) C54-$TiSi_2$ NWs	2−10 μm	898−973	–[b]	–[b]	–[b]	–[b]

sample from this study	morphologies and phases	NWs Length/ Film Thickness	temperature (K)	time (min)	E_o (V μm^{-1})	β	J_{max} (μA cm^{-2})
I	TiSi NWs on C54-$TiSi_2$ film	2−5 μm/10.5 μm	1073	60	5.25	876	0.48
II	partial C54-$TiSi_2$ film	–[b]	1073	10	–[c]	–[c]	–[c]
III	short TiSi NWs on C54-$TiSi_2$ film	0.5−3 μm/8 μm	1073	30	8.5	418	0.07
IV	C54-$TiSi_2$ film	2.6 μm	973	60	10.4	343	0.014
V	Ti_5Si_3 NWs on C54-$TiSi_2$ film	2−5 μm/6 μm	973	360	5.4	816	0.18

[a] The E_o is defined as the current density reaches 1 μAcm^{-2}. [b] Not reported. [c] Partially formed $TiSi_2$ film does not emit electrons.

experimental parameters for samples investigated in this study are summarized in Table 1.

2.2. Instruments for Characterizations. Scanning electron microscopic (SEM) images and energy dispersive X-ray spectra (EDX) of the samples were taken with a Hitachi S-4700I and a JEOL JSM-7401F operated at 15 keV. High-resolution transmission electron microscopic (HRTEM) images and EDX were acquired on a scanning transmission electron microscope (STEM) JEOL JEM-3000F at 300 kV. A cross-sectional TEM sample was prepared using a dimpling and ion milling technique.[61] X-ray diffraction (XRD) patterns of the samples were obtained using a Bruker AXS D8 ADVANCE with Cu Kα1 radiation.

EFE measurements were carried out using a home-built apparatus, composed of a vacuum chamber and a spherical-shaped tungsten probe (diameter 1 mm) as the anode. The sample-to-anode distances were adjustable by a manipulator equipped with a micrometer. All measurements were taken below 1.05×10^{-3} Pa at room temperature. Current-to-voltage ($I-V$) characteristics were measured using a Keithley 237 or 2410. The maximum applied voltage was 1100 V while the current was restricted to 10 mA. Sheet resistances of the samples were measured by a four-probe method using a Mitsubishi MCP-T600 resistivity meter.

3. Results and Discussion

In a typical reaction, $TiCl_4$ was vaporized into a hot-wall LPCVD reactor loaded with Ti powders at the heating zone at 1173 K, which was upstream from Si (100) substrates placed at the center heating zone at 973−1073 K. The reaction between $TiCl_4$ and Ti generated gaseous titanium subchlorides $TiCl_x$, which would undergo disproportionation to regenerate $TiCl_4$ and to deposit Ti.[62] Depending on the reaction time employed, from 10 min to 6 h, growth of products composed of gray to black thin films on the substrates was observed. In Table 1, effects of varying the reaction parameters on morphology and phase of the products are summarized.

(61) Weaver, L. *Microsc. Res. Tech.* **1997**, *36*, 368.
(62) Lee, C.-Y. *Chem. Vap. Deposition* **1999**, *5*, 69.

In this report, we will discuss more on characterizations of the samples deposited at 1073 K, including **I** and **III**, the vertically grown long and short single crystalline TiSi NWs, respectively. We will not focus on samples grown at 973 K, C54-$TiSi_2$ thin film (**IV**) and Ti_5Si_3 NWs (**V**) because we have reported their fabrications in the previous communication already.[36]

3.1. SEM Characterizations. SEM images of **I** are shown in Figure 1. Figure 1a is a low magnification top-view image of **I**, revealing the presence of high density 1-D nanostructures on the deposited product. The EDX spectrum shown in the inset of Figure 1a suggests that **I** is composed of Ti and Si only. A high magnification image in Figure 1b shows that the 1-D nanostructures are NWs with diameters of 30−80 nm. We do not observe metal particles on the tips of the NWs. This suggests that the NWs were not grown via a vapor−liquid−solid (VLS) mechanism.[63] Figure 1c displays a side-view image of **I**, indicating that the product deposited on the substrate is composed of a film (thickness 10.5 μm) and above it, a layer of NWs pointing upward. An enlarged side-view image of the NWs in Figure 1d shows that the NW lengths are 2−5 μm.

Figure 2 displays the images of **II**−**V**, the products prepared at different conditions. When the growth time was 10 min, sample **II** was obtained. As shown in Figure 2a, the Si substrate is partially covered (ca. 20%) by irregularly shaped islands with areas of tens to hundreds of μm^2. Unlike sample **I**, we could not find the presence of any 1-D nanostructure on the substrate of **II**. The rugged surface islands, shown in the side-view SEM image in the inset of Figure 2a, imply that they might be formed by etching and deposition reactions involving the Si surface and the gaseous $TiCl_x$ molecules.[64,65] Figure 2b

(63) Wagner, R. S.; Ellis, W. C. *Appl. Phys. Lett.* **1964**, *4*, 89.
(64) Reynolds, G. J.; Cooper, C. B.; Faczl, P. J. *J. Appl. Phys.* **1989**, *65*, 3212.
(65) Southwell, R. P.; Seebauer, E. G. *J. Vac. Sci. Technol., A* **1995**, *71*, 5918.

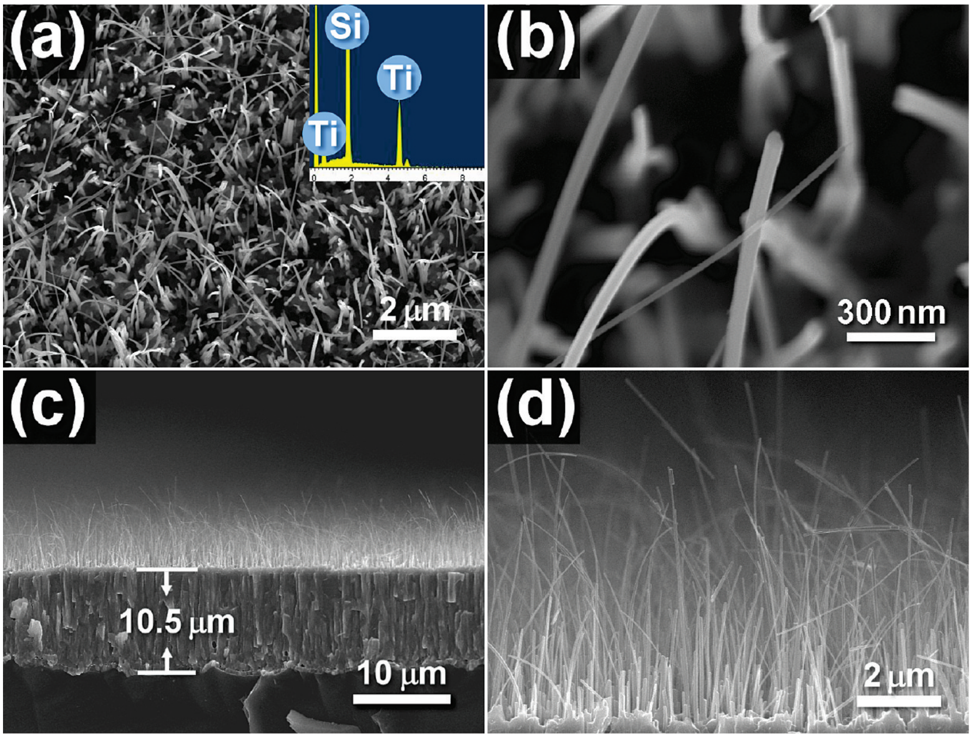

Figure 1. SEM images of **I** grown on Si. (a) Top-view and EDX (inset), (b) high magnification image, (c) low magnification side-view, and (d) high magnification side-view image.

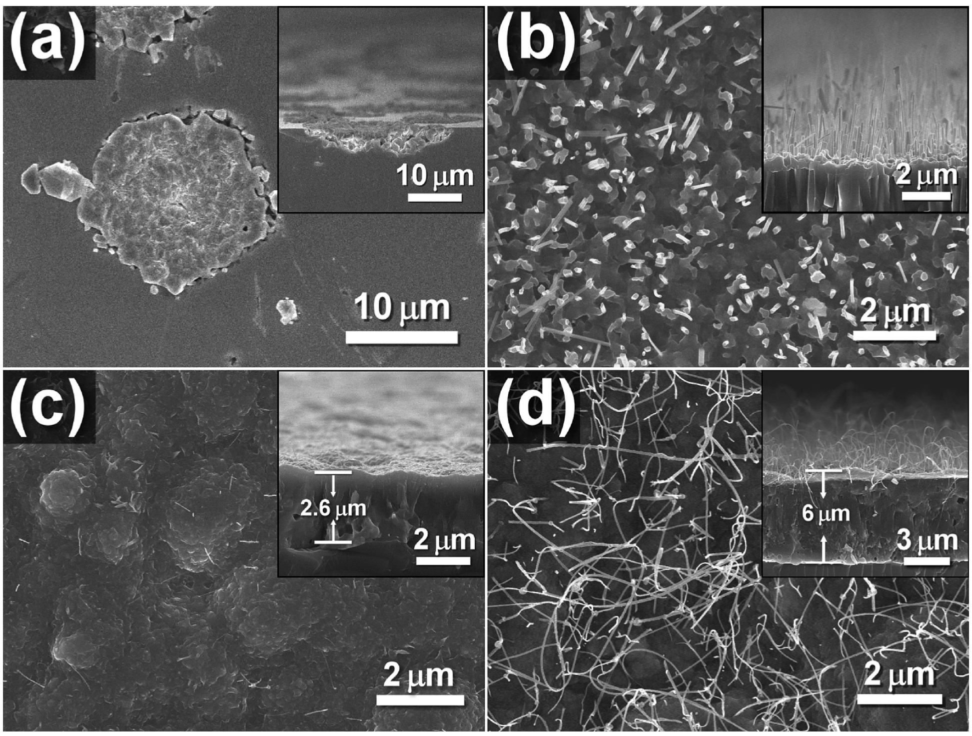

Figure 2. SEM top-view and side-view (inset) of (a) **II**, (b) **III**, (c) **IV**, and (d) **V**.

shows the image of sample **III**, obtained after the reaction was carried out for 30 min at 1073 K. Growth of numerous NWs with lengths 0.5−3 μm on top of a thin film with a thickness of 8 μm is observed. Comparing samples **I**−**III**, we conclude that only a thin film was grown at the early stage of the reaction. After a certain period of time, NWs started to grow on the film. As the reaction time was lengthened, density and length of the NWs increased accordingly.

The SEM image (Figure 2c) of sample **IV**, which was grown at 973 K for 1 h, shows the presence of few and scattered NWs on a layer of thin film.[36] When the growth

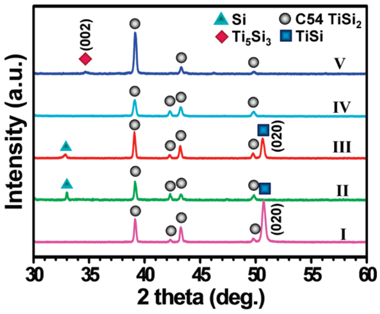

Figure 3. XRD patterns of **I**−**V**. Assignment of peaks: ●, C54-$TiSi_2$; ■, TiSi (020); ♦, Ti_5Si_3 (002); ▲, Si (020), this forbidden signal only appears in several samples grown on a specific batch of Si substrates. For clarity, Si (400) at 69.2° is not shown.

time was extended, the NWs elongated as well. For example, Figure 2d demonstrates the image of sample **V**, which was grown at 973 K for 6 h. It displays the growth of abundant thread-like NWs, diameter ca. 20−50 nm and length up to several micrometers, on top of a thin film. The above observations suggest that, before the growth of 1-D titanium silicide NWs (characterization of the products by XRD and TEM will be discussed below), an adequate reaction time was required to allow the initial deposition of a layer of titanium silicide thin film on the Si substrate.

3.2. XRD Characterizations. XRD patterns of the samples **I**−**V** are shown in Figure 3. All of them display four diffraction peaks marked by gray circles at 2θ = 39.1°, 42.2°, 43.2°, and 49.7°. This set of peaks indicates the presence of orthorhombic C54-$TiSi_2$ (JCPDS 35-0785) as the major product. Since all of the samples have a layer of thin film several micrometers thick, we conclude that all of the thin films are composed of C54-$TiSi_2$. In addition to the C54-$TiSi_2$ pattern, sample **I** shows a strong peak at 2θ = 50.3°, which is marked by a blue square in Figure 3. This signal is also observed for **III**, the sample with short NWs, but not for **II**, which does not show any 1D nanostructure in the SEM image. The peak is assigned to the reflection from {020} plane of orthorhombic TiSi (JCPDS 17-0424). In Figure S2a in the Supporting Information, a detailed XRD scan of **I** taken at 2θ = 25 - 38° was demonstrated. The diffraction peaks observed at 2θ = 32.83°, 35.3°, and 36.93° were indexed to be the reflections from TiSi {201}, {002}, and {210} planes, respectively. Thus, we conclude that in **I**, the NWs on top of the thin film, as shown in Figure 1, are composed of TiSi. These data differ slightly from the standard XRD pattern of TiSi. We suggest that unlike randomly oriented TiSi crystals in powders, **I** contains TiSi NWs with a preferred growth orientation in [020] direction. This is further confirmed by TEM studies and will be discussed below. All samples also showed a very strong signal at 69.2°. This was assigned to Si {400} planes from the substrates. For clarity, it is not displayed in Figure 3 (see Figure S2b for a pattern of **I** with the substrate signal). For sample **IV**, only diffraction peaks of C54-$TiSi_2$ are observed. Accordingly, **IV** is determined to be a film composed of C54-$TiSi_2$. For sample **V**, in addition to the pattern of C54-$TiSi_2$, a weak diffraction peak at 2θ = 34.8° is shown. This is assigned to the reflection by {002} plane of Ti_5Si_3 (JCPDS 78-1429), the main component of the NWs in **V**. The XRD observation is in good agreement with the TEM result, which indicates that the preferred growth direction of the NWs is along [002] axis of Ti_5Si_3.[36] We speculate whether isolated Ti and Si crystals could be grown during the reactions because $TiCl_x$ and $SiCl_x$ byproducts were known to deposit thin films in their elemental forms.[62,66] However, the XRD results do not show any peak which can be assigned to Ti and Si crystals.

3.3. TEM Studies of TiSi NWs. Figure 4a displays a representative TEM image of a section of a single NW obtained from **I**. The sample has a diameter ca. 80 nm and a length ca. 1 μm. The selected-area electron diffraction (SAED) pattern in Figure 4b, taken from the circled region in Figure 4a, suggests that the NW is single crystalline. The observed spots are determined to be from {200}, {210}, and {010} planes of orthorhombic TiSi with [001] zone axis. In Figure S3 in the Supporting Information, the results from another NW, with dimensions similar to those of the one displayed in Figure 4, were shown. The SAED pattern in Figure S3c in the Supporting Information also confirmed that the NW was single crystalline. The diffraction spots were determined to be from {010}, {011}, and {001} planes of orthorhombic TiSi with [100] zone axis. From Figures 4c and S3c (in the Supporting Information), the lattice parameters *a*, *b*, and *c* are calculated to be 0.65, 0.36, and 0.49 nm, respectively. They are close to the values of TiSi (JCPDS 17-0424), 0.654, 0.364, and 0.499 nm, respectively. Figure 4c exhibits the HRTEM image from the same region. The estimated lattice spacings 0.16, 0.24, and 0.18 nm are assigned to {400}, {210}, and {010} planes, respectively. From the HRTEM image shown in Figure S3d (in the Supporting Information), the observed lattice spacings 0.36 and 0.49 nm were assigned to {010} and {001} planes, respectively. From the HRTEM images, *a*, *b*, and *c* are determined to be 0.64, 0.36, and 0.49 nm, respectively. An STEM image and the corresponding EDX line-scan profiles of an NW are shown in Figure 4d. The data indicates that the NW is mainly composed of Ti and Si, which distribute uniformly along the NW cross-section. A trace of residual O atoms, probably originated from the TEM sample preparation, is also observed. On the basis of the results from the XRD and the TEM studies, the NWs in **I** are determined to be single crystalline TiSi with a preferred growth in [010] direction. Since an NW from sample **III** showed TEM data identical to those shown in Figure 4, we conclude that the NWs in **III** were single crystalline TiSi also. On the other hand, using the TEM result of an NW in **V**, we determined that it was a single crystalline titanium rich silicide, Ti_5Si_3, grown preferentially along the [001] direction.[36]

(66) Mendicino, M. A.; Seebauer, E. G. *J. Electrochem. Soc.* **1993**, *140*, 1786.

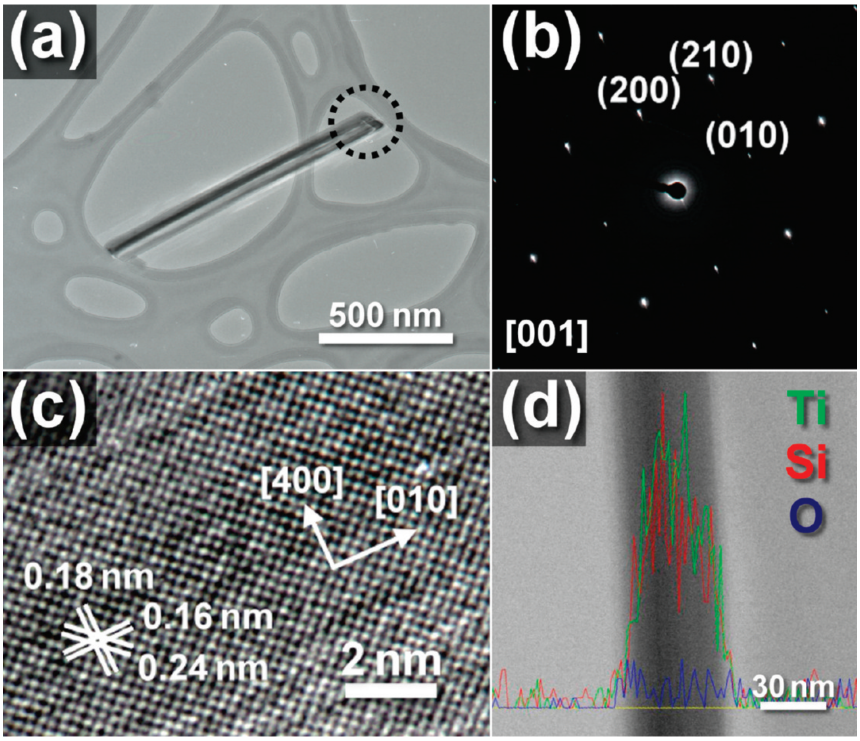

Figure 4. (a) TEM image of a NW isolated from **I**, (b) SAED pattern and (c) HRTEM image from the circled region in (a), and (d) TEM and EDX elemental line profiles of another NW from **I**.

3.4. Characterization of the Interface between TiSi NWs and C54 $TiSi_2$ Film. From cross-sectional SEM images of **I** (Figures S4a and S4b in the Supporting Information), a layer of thin film, with a slightly different contrast and a thickness ca. 600 nm, was observed between the NWs and the C54-$TiSi_2$ film deposited on the Si substrate. This phenomenon was also observed for sample **V**. On the other hand, sample **IV**, which was a C54-$TiSi_2$ film, did not show such a layer, as shown in Figures S4c and S4d in the Supporting Information. EDX analyses of the interlayers and the films of **I** and **V** were carried out at the spots shown in Figure S5 in the Supporting Information. The Ti contents of the interlayers were higher than those of the films below. In addition, the Ti/Si ratios of the interlayers of **I** and **V** were 0.88 and 1.57, respectively. The chemical compositions of both interlayers coincided well with those of the NWs grown on top of them. Thus, it appears that the composition and the crystal structure of the NWs are highly influenced by the interlayers. Furthermore, the EDX line-scans of **I** and **V** in Figure S6 (in the Supporting Information) revealed that the Si contents of the interlayers were lower than those of the films below them.

The interlayer between the NWs and the silicide film may provide clues to explain how and why the NWs grew in this study. Therefore, we carried out a TEM investigation of the interlayer of **I**. A thin slice of cross-section of **I** was prepared by the use of the dimpling and ion milling technique.[61] In Figure S7 in the Supporting Information, presence of vertically grown NWs on the bottom film was shown. Unfortunately, this region was too thick for detailed HRTEM and SAED characterizations. Figure S8 in the Supporting Information demonstrated TEM studies from another area on the slice. This region was thin enough for detailed investigations. Except a couple of NW roots, all the NWs on the slice were removed in the polishing process. A layer with a thickness of 20−200 nm and uneven boundary was observed in the upper regions in Figures S8a and S8b in the Supporting Information. The apparent variation of the film thickness could be the results of the irregular nature of the interlayer and the uneven processing during the sample preparation. An area of the thin layer was selected for detailed investigations (Figure S8b in the Supporting Information). A high magnification TEM image of this area is displayed in Figure 5a. It shows a top layer with a thickness ca. 10 nm. The HRTEM image (Figure 5b) of the rectangular area in Figure 5a displays the image near the interface. An amorphous layer on top of a crystalline layer can be observed. In the lower crystalline region, two sets of lattice spacings are clearly seen and are measured to be 0.23 and 0.20 nm. These coincide well with (311) and (022) lattice spacings of C54-$TiSi_2$, respectively. Figure 5c displays the result of an SAED study of the rectangular area shown in Figure 5a. The dotted pattern suggests that the single crystalline region could be indexed to [011] zone axis of orthorhombic C54-$TiSi_2$. Figure 5d,e presents the EDX spectra acquired from areas in the circle and the dotted circle in Figure 5a, respectively. The spectra confirm that both the amorphous and the crystalline regions are mainly composed of Ti and Si. Clearly, the Ti/Si ratio of the amorphous layer is higher than that of the crystalline layer below. This is consistent with the EDX line-scan result shown in Figure S6 in the Supporting Information.

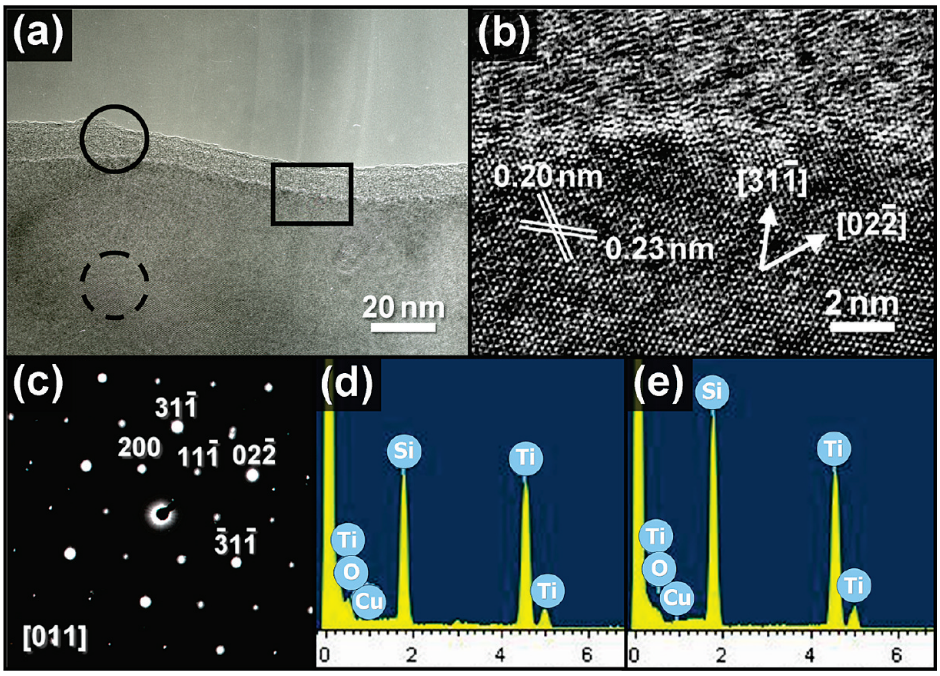

Figure 5. (a) Cross-sectional TEM image of the interface in **I**, (b) HRTEM image and (c) SAED pattern from the solid square region in (a). EDX spectra from (d) the solid and (e) the dotted circled areas in (a). The Cu signal is from the Cu TEM grid.

Thus, we designate the amorphous layer to have a composition $TiSi_{2-x}$, where $0 < x < 1$. This is due to the fact that along the growth direction of the layers, the Ti concentration increases while the Si concentration decreases as the reaction proceeds. Moreover, a high magnification image of the interlayer shown in Figure S8d (in the Supporting Information) indicated the presence of small crystallites. Enlarged views of some crystallites were shown in Figure S9 in the Supporting Information. All of them displayed lattice spacings assignable to crystal planes of TiSi. Consequently, the presence of the nanocrystallites in the interlayer appears to be the key factor to induce the growth of NWs with phases different from the C54-$TiSi_2$ thin film below. Previous studies involving solid state diffusion systems have reported that amorphous titanium silicide layers at the Ti/Si interface formed before the formation of crystalline slilicides.[67] Thus, the growth sequence of the silicide layers are determined to be in the order: growth of a $TiSi_2$ thin film on Si initially, formation of an *a*-$TiSi_{2-x}$ interlayer next, nucleation of TiSi in the interlayer subsequently, and lengthening of TiSi NWs finally. How and why the presence of the interlayer initiates the NW growth will be discussed further below.

3.5. Growth Pathway of TiSi NWs. On the basis of the data presented above, a reaction pathway is proposed in Scheme 1 to summarize the TiSi growth. In our CVD system, $TiCl_{4(g)}$ reacts with Ti powders to produce $TiCl_x$ subhalides at 1173 K in the first heating zone upstream from the Si substrate. Then, as the $TiCl_x$ molecules reach the substrate surface at 1073 K, they disproportionate into $TiCl_4$ molecules and Ti atoms, which deposit on the substrate surface.[62] The Ti atoms could react with the Si substrate directly to form titanium silicides, such as C54-$TiSi_2$ produced in this study. Alternatively, vapors of $TiCl_4$ and $TiCl_x$ could react directly with the Si substrate to produce titanium silicides and $SiCl_x$ byproducts. $SiCl_x$ may decompose and act as another source of Si atoms for the silicide formation. After the $TiSi_2$ film grows to a certain thickness, this relatively thick and inert layer may act as a barrier to impede diffusion of Si atoms from the substrate.[68] This would hamper further interaction between the Si atoms in the substrate and the Ti atoms deposited on the surface. Consequently, the Si concentration on the surface is reduced while formation of a Si-poor *a*-$TiSi_{2-x}$ interlayer begins. We want to emphasize that the interlayer, which may be viewed as a quasi-liquid thin film, might be the key to the successful growth of titanium silicide NWs in this study.[69] After the amorphous interlayer is formed, nucleation of crystallites of a different titanium silicide phase, such as TiSi in **I** and **III**, as well as Ti_5Si_3 in **V** may start. Chemical composition of the interlayer, which varies with the reaction condition, affects the phase nucleated.[70] As the reaction proceeds, these nuclei at a relatively low supersaturation condition act as the seeds for further growth of the single crystalline titanium silicides. Since quantity of the seeds is limited, sites suitable for silicide growth are limited as well. Consequently, the crystalline NWs can grow only from selected spots on top of the amorphous layer. Reports on how quasi-liquid layer affected crystal growths are known. Recently, several research groups demonstrated the fabrication of NWs of metal silicide, including $NiSi_x$, $CrSi_2$, FiSi, and CoSi, without the use of any metal

(67) Chen, L. J. *Mater. Sci. Eng., R* **2000**, *29*, 115.

(68) Southwell, R. P.; Seebauer, E. G. *J. Electrochem. Soc.* **1997**, *144*, 2122.
(69) Luo, J. *Crit. Rev. Solid State* **2007**, *32*, 67.
(70) Wang, M. H.; Chen, L. J. *Appl. Phys. Lett.* **1991**, *59*, 2460.

Scheme 1. Proposed Growth Pathway of the TiSi NWs[a]

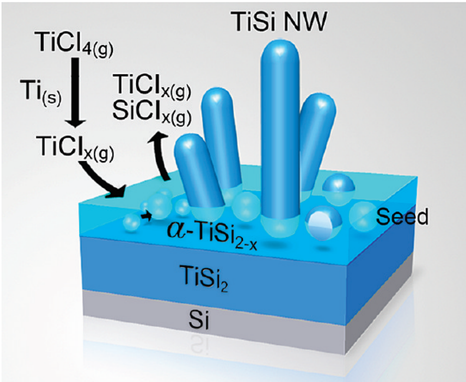

[a] *x* denotes variables.

nanoparticles.[41,46,48,58] These may proceed via analogous routes.

Reaction temperature has a great influence on the crystal phase and the morphology of the NWs grown in this study. We suggest that the phase of the obtained NWs is highly dependent on the elemental composition of the interlayer. At a high temperature, the diffusion rate of Si atoms from the substrate is raised.[71] This would increase the Si concentration in the interlayer, as verified in the SEM EDX data shown in Figure S5 in the Supporting Information. In addition, the disproportionation of $TiCl_{x(g)}$ to form $TiCl_{4(g)}$ and $Ti_{(s)}$ is less favored because the estimated Gibbs free energy of reaction is more positive.[72] All of these would allow the interlayer formed at 1073 K to contain more Si than that deposited at 973 K. Consequently, the NWs grown at 1073 K have more Si atoms to form the TiSi phase, while the NWs obtained at 973 K, with less Si atoms, have the Ti_5Si_3 phase. The distinct morphologies of the NWs may result from the difference in their diameters, which are 30−80 nm and 20−50 nm for TiSi and Ti_5Si_3, respectively. In addition, the bulk mechanical hardness of TiSi and Ti_5Si_3, 18.0 and 9.86 GPa, respectively, may affect their morphology too.[28] Besides, Ti_5Si_3 NWs may contain more defects and become thread-like, whereas the TiSi NWs might be better crystallized so that the NWs grow upward on the substrate. All of the factors may explain why the TiSi NWs are straight while the Ti_5Si_3 NWs are coiled.

As mentioned in the TEM studies, the TiSi NWs show preferred growth orientation in the [010] direction while the Ti_5Si_3 NWs show that in the [001] direction. We analyzed their crystal structures to rationalize the observed phenomena. Figures S10 and S11 in the Supporting Information displayed the crystal models of TiSi and Ti_5Si_3 viewed along *a*, *b*, and *c* axes. In Figure S10 in the Supporting Information, the Si−Si distance found in the structure was 0.2171 nm. Clearly, this is much smaller than the Si−Si distances of many molecular compounds containing Si−Si single bonds, ranging from 0.2363 to 0.2370 nm.[73,74] On the other hand, the Ti−Si and the Ti−Ti distances shown in Figure S10 in the Supporting Information were 0.2599 and 0.3227 nm, respectively. They are longer than the Ti−Si and the Ti−Ti bond distances reported in the literature for the corresponding molecular compounds, 0.2594−0.2629 nm and 0.2889−0.2942 nm for the Ti−Si and the Ti−Ti bonds, respectively.[75,76] This suggests that the Si−Si bonds in TiSi are stronger than the Ti−Si and Ti−Ti bonds. Consequently, forming Si−Si bonds stabilizes the structure more than forming Ti−Si and Ti−Ti bonds does. In Figure S10 in the Supporting Information, the presence of high density Si−Si bonds along *b* axis of TiSi was observed. This suggests that the growth of TiSi along the [010] direction should be more favored because the overall energy is decreased. A similar analysis is carried out to account for the preferred growth of hexagonal Ti_5Si_3 in the [001] direction. Figure S11 in the Supporting Information displayed the crystal models of hexagonal Ti_5Si_3 viewed along *a* and *c* axes. Formation of Ti chains with an extremely short Ti−Ti distance 0.2575 nm was observed along *c* axis. The distance is shorter than the Ti−Ti distances observed for many molecules containing Ti−Ti bonds. The nearest Si−Si and Si−Ti distances were 0.3024 and 0.2797 nm, respectively. These are longer than the molecular Si−Si and Ti−Si bond distances mentioned above. As a result, the growth of Ti_5Si_3 along the [001] direction would produce more Ti−Ti bonds and lower the energy. For comparison, the growth directions of hexagonal phase $CrSi_2$ and Fe_5Si_3 NWs were also found to be along [001].[41,47] On the other hand, the reported growth directions of TiSi NPs and NWs were different from our observation.[35] After comparing the XRD results, we discover that the reported nanostructures had a different TiSi phase (JCPDS-65-2585, ICSD 20375).

3.6. Electron Field Emission Properties of Titanium Silicide Samples. Titanium silicides are suitable for EFE applications, due to their high melting points, low work functions (3.71−4.53 eV), and high conductivities.[1,28] Thus, EFE properties of the samples obtained in this study were investigated. The results are shown in Figure 6. Detailed EFE properties, such as turn-on field E_o, which is defined as the electric field required to generate a current density (J) of 10 μA cm^{-2}, and field enhancement factor β, which is deduced from the Folwer-Nordheim (F-N) plot (the inset of Figure 6 showing the $\ln(JE^{-2})-(E^{-1})$ relationship), are summarized in Table 1.[36] Sample **I** demonstrates the best EFE performance among our samples. The E_o of **I** is low, only 5.25 V μm^{-1}, while the J_{max} (at an applied voltage 1100 V) is high, 0.48 mA cm^{-2}. The low E_o value is associated with its high NW aspect ratio. The high J_{max} could be attributed to its high NW

(71) Gossmann, H. J.; Rafferty, C. S.; Luftman, H. S.; Unterwald, F. C.; Boone, T.; Poate, J. M. *Appl. Phys. Lett.* **1993**, 63.
(72) Reaction-Web, Facility for the Analysis of Chemical Thermodynamics; CRCT, Ecole Polytechnique de Montréal, Montréal; http://www.crct.polymtl.ca/fact/.
(73) Chisholm, M. H.; Chiu, H.-T.; Folting, K.; Huffman, J. C. *Inorg. Chem.* **1984**, *23*, 4097.
(74) Stueger, H.; Fuerpass, G.; Renger, K.; Baumgartner, J. *Organometallics* **2005**, *24*, 6374.
(75) McAlexander, L. H.; Hung, M.; Li, L.; Diminnie, J. B.; Xue, Z.; Yap, G. P. A.; Rheingold, A. L. *Organometallics* **1996**, *15*, 5231.
(76) Thorn, M. G.; Vilardo, J. S.; Lee, J.; Hanna, B.; Fanwick, P. E.; Rothwell, I. P. *Organometallics* **2000**, *19*, 5636.

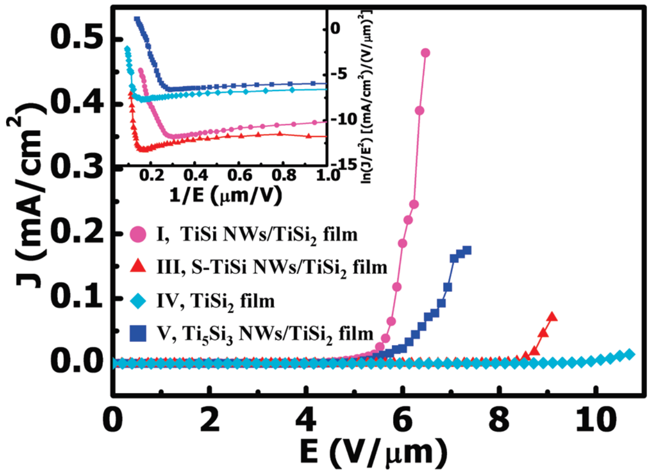

Figure 6. EFE current density as a function of applied electric field of samples **I** and **III**−**V**. Inset shows their corresponding Fowler-Nordheim plots.

density, low TiSi resistivity, and low sheet resistance, which is 8.6×10^{-2} Ω/□. β of **I** is 876, calculated from the equation $\beta = \phi^{3/2}/\phi_e$, where ϕ is the work function of TiSi, 3.99 eV, while ϕ_e is the effective work-function derived from the slope of the F-N plot of **I** shown in the inset of Figure 6.[77] Other samples from this study did not perform equally well because they lack the proper combination of NW density, aspect ratio, and overall NW/thin film resistance. For example, **II** could not emit electrons even under the highest possible field applied. This is because **II** was a partially formed $TiSi_2$ film lacking 1-D nanostructures for emission. Sample **III** shows an E_o 8.5 V μm^{-1} which is higher than **I**'s value because **III** has shorter NWs and, consequently, a lower aspect ratio. The same reason is also applicable to explain **IV**'s poor performance. Sample **V** has an E_o 5.4 V μm^{-1}, which is slightly higher than **I**'s result, but a J_{max} only a third of the value of **I**. This is attributed to **V**'s low NW density, high Ti_5Si_3 resistivity, and high sheet resistance, 1.9×10^{-1} Ω/□. In contrast, **I** is composed of high density, high aspect ratio, and vertically aligned crystalline TiSi NWs. These ensure that nearly all NWs in **I** could emit electrons effectively. The result is that **I** is one of the best titanium silicide NW emitting materials reported so far.[5,6]

(77) Fowler, R. H.; Nordheim, L. W. *Proc. R. Soc. London, Ser. A* **1928**, *119*, 173.

Conclusion

In conclusion, TiSi NWs were grown vertically on a C54-$TiSi_2$ film employing a unique CVD process. Disproportionation of gaseous $TiCl_x$ subhalides, formed by reacting $TiCl_{4(g)}$ and $Ti_{(s)}$ at high temperatures, provided Ti atoms while the Si substrate supplied Si atoms. Presence of an amorphous $TiSi_{2-x}$ interlayer was observed between the NWs and the film. This interlayer, probably existing as a quasi-liquid thin film during the growth, appears to be the key factor to assist the development of 1-D nanostructures. Varying the reaction conditions, such as time and temperature, would modulate reactivity and diffusion rate of the Ti and Si containing reactive species and limit the number of nucleation sites. This would influence not only composition and morphology but also physical and chemical properties of the product. Growth direction of the TiSi NWs was determined to be along [010]. The phenomenon could be attributed to the presence of strong Si−Si bonds along TiSi's *b* axis. This would lower the energy and provide high stability for the growth of TiSi in [010]. The vertically grown TiSi NWs demonstrate superior EFE properties with a low E_o 5.25 V μm^{-1} and a high β 876. The high performance is attributed to TiSi's low work function, growth of high density, high aspect ratio, and vertically aligned 1D nanostructures and the existence of a highly conductive $TiSi_2$ film below. Our study has provided a new route to grow unusual TiSi NWs which cannot be fabricated by other means so far. The synthesis will offer opportunities to study other physical and chemical properties of this unique material in the future.

Acknowledgment. We are grateful to the support from the National Science Council, "Aim for the Top University Plan" of the National Chiao Tung University and the Ministry of Education of Taiwan, the Republic of China. We also thank Ming-Cheng Wu and Professor Chi-Shen Lee for helpful discussions.

Supporting Information Available: Experimental setup of the CVD system, XRD and ED patterns, EDX data, and SEM, TEM, and crystal structure images (PDF). This material is available free of charge via the Internet at http://pubs.acs.org.